

## Evaluation of the Biological Activity of Manganese oxide-Nanoparticles as antibacterial *Staphylococcus aureus*

Sarab morad<sup>1</sup>, Laith A. Yaaqoob<sup>2</sup>

<sup>1,2</sup>Department of Biotechnology, College of Science, University of Baghdad, Iraq

Corresponding Author Email: [Sarab.morad1106a@sc.uobaghdad.edu.iq](mailto:Sarab.morad1106a@sc.uobaghdad.edu.iq)

Supervisor Email: [Laith.yaaqoob@sc.uobaghdad.edu.iq](mailto:Laith.yaaqoob@sc.uobaghdad.edu.iq)

### Abstract

Pathogenic strains frequently spread infections by producing virulence factors like potent protein toxins and the expression of a cell-surface protein that binds and inactivates antibodies. *Staphylococcus aureus* is one of the leading pathogens for deaths linked to antimicrobial resistance and the emergence of antibiotic-resistant strains. There is currently no licensed *S. aureus* vaccine, despite extensive research and development. Therefore, the aim of this study includes biosynthesis of Manganese oxide-nanoparticles (MnO-NPs) using *Lepidium sativum* aqueous plant leaves extract, and use of the biosynthesized nanoparticles as antibacterial and antibiofilm against multi-drug resistant *S. aureus*. 150 samples of both sexes, ranging in age from 1 to 60 years, were randomly selected from 65 male and 85 female patients who had infected burns and wounds at various hospitals. After the final diagnosis of the clinical samples, 20 isolates of *Staphylococcus aureus* were obtained, then full identification of *S. aureus* using conventional biochemical tests. The antibiotic susceptibility test for fourteen antibiotics was performed by the standard well diffusion method, The results of the current investigation revealed that all *S. aureus* isolates varied in their resistance to the 14 antibiotics utilized in this study. Therefore, ten multi-drug resistant isolates of *S. aureus* were selected and examined their ability to form biofilm using the micro-titer plate method; the results revealed that eight isolates were strong in biofilm formation and two isolates were moderate. Maceration method was used to prepare *Lepidium sativum* aqueous plant leaves extract. Furthermore, MnO-NPs were prepared from the *Lepidium sativum* aqueous plant leaves extract and diagnose using ultraviolet (UV) spectroscopy, Field emission Scanning electron microscopy (FE-SEM), atomic fluorescence microscopy (AFM), X-ray scattering (XRD) and Fourier transformation infrared spectroscopy (FTIR). In addition, several experiments were conducted on the nanoparticles, including evaluation of antibacterial activity, biofilm formation and determination of the minimum inhibitory concentration.

The diagnostic results showed that the nanoparticles are spherical in shape, single or combined, and crystalline for MnO-NPs and an average size of 27.69 nm. As the results showed that the MnO-NPs in concentration of 64 mg/ml was more effective than the MnO-NPs in concentration of 32 mg/ml, which gave the highest inhibition zone value of 19.67 mm. Furthermore, The result of the minimum inhibitory concentration (MIC) values of MnO-NPs on *S. aureus* isolates were 1, 2 and 4 mg/ml in various isolates. The results of the anti-biofilm activity on *S. aureus* isolates showed the MnO-NPs inhibit 100% biofilm formation in concentration 1 mg/ml.

From the results obtained in this study, several conclusions were concluded as the following, *Staphylococcus aureus* isolates showed high resistance to All antibiotics used in the study. It can also synthesize of MnO-NPs by extracted from *Lepidium sativum* aqueous plant leaves, and the synthesized MnO-NPs have significant antibacterial *S. aureus* agent, it also inhibits of the formation biofilms in *S. aureus* depending on the concentration used.

More studies should be conducted about the antibacterial activities of MnO-NPs on the other microorganisms associated with different human infections, and conduct more studies of MnO-NPs on immunological and cancer cell lines due to their effectiveness as an antioxidant.

**Keywords:** MnO-nanoparticles, antibacterial activity, *Lepidium sativum*, FTIR, AFM, FE-SEM, UV and XRD.

### Introduction

Resistance to antibiotics and antifungal drugs in pathogenic bacterial and fungal species has become a serious worldwide issue [1]. The production of biofilms by these microbes is a crucial factor in why antimicrobial medications are ineffective [2]. These dangerous microbial in biofilm form can tolerate a

thousand doses of traditional antibacterial drugs [3]. In this case, nanotechnology has arisen and taken the lead in designing nanoscale materials to address the problem of antibiotic resistance.

Materials with a nanostructure have been employed for their efficacy, durability, and efficiency. Due to their increased surface area to size ratio, these materials are often employed in biological, physical,

chemical, pharmaceutical, engineering, and environmental sciences [4]. Several physical and chemical techniques can be used to create nano-based materials, also known as nanoparticles (NPs). These procedures are typically expensive, inefficient, and bad for the environment. The advantages of using green or biological processes over traditional chemical, physical, or other industrial processes are directly related to effectiveness, affordability, environmental friendliness, and reusability. Making metal and metal oxide nanoparticles is one of green chemistry's most important applications in chemical, pharmacological, biological, and other disciplines [5].

Due to their numerous beneficial physical, chemical, and biological features, metal and metal oxide nanoparticles have recently received significant attention. The majority of these inorganic nanoparticles are recognized for their use in the chemical, biological, pharmaceutical, and electrical sectors. Using any readily accessible biomaterials to create nanoparticles in a green manner is a suitable alternative to more traditional processes [6]. The MnO-NPs have a wide range of uses in several scientific and technological domains. Generally speaking, MnO-NPs are employed in sensors, energy storage, catalysis, environmental remediation, and antibacterial activities [7].

#### **Materials and methods**

##### **Synthesize of manganese oxide-nanoparticles by *Lepidium sativum* aqueous plant leaf extract**

##### **Preparation of *Lepidium sativum* aqueous plant leaf extract**

The *Lepidium sativum* plant leaves were removed, carefully cleaned, and chopped into small pieces. Then, 100 g of leaves were soaked with 500 ml of distilled water at 60 °C for 4 to 5 hours. The extract was then filtrated using a centrifuge for ten minutes at 10,000 rpm; the filtrate was used to prepare NPs [8].

##### **Synthesize of manganese oxide-nanoparticles**

All substances and reagents employed in the manufacture of MnO-NPs were bought from Sigma, Ltd, UAS, and the process given by Ezhilarasia *et al.* [9], 1000 gram of young plant (*Lepidium sativum*) clean and mixed with distilled water in (60 °C) for 5 hours. Then mixing very well with blender (fruits mixer) and leave it 24 hours in room temperature. the extract was then filtrated using a centrifuge for ten minutes at 10,000 rpm. the liquid filtrate will be ready for prepare manganese oxide-nanoparticles. 25gram of manganese (II) sulphate (MnSO<sub>4</sub>.H<sub>2</sub>O) was dissolved in 250 ml of plant leaf extract and dispersed by an ultra-sonication bath for 10 minutes. The extract placed

in a beaker glass for 24 hours inside the shaker the extract was then filtrated using a centrifuge for ten minutes at 10,000 rpm. The precipitate was collected and placed in glass dishes in an incubator for 48 to 72 hours in order to dry and grind it, thus the nanoparticles was ready to use. Then, various concentrations of the synthesized MnO-NPs were prepared.

#### **Nanoparticles Characterization Techniques**

UV-Visible Absorption Spectroscopy (UV-VIS) double-beam spectrophotometers were used to measure the absorbance spectra of the MnO-NPs solution. Atomic force microscopy (AFM) measurements of the average diameter crystalline size were used to show the generated MnO-NPs 2D and 3D topologies. Field emission scanning electron microscopy (FE-SEM) was used for further characterization. The X-ray diffraction patterns were used to determine the crystal structure (XRD). Fourier transformation infrared spectroscopy (FTIR) (Shimadzu) analysis was utilised to investigate the characterization of functional groups on the surface of MnO-NPs by plant extracts. As per standard procedures, the samples were created by spreading them out on a glass slide. Following that, the sample was examined; the preparation of MnO-NPs was performed in the Biotechnology Department, Nanotechnology Laboratory / College of Science / University of Baghdad / Iraq, while the characterization was conducted in the Chemistry Department / College of Science / University of Baghdad / Iraq.

#### **Evaluation of antibacterial activity**

##### **Preparation of bacterial isolates**

In this study, the isolated bacteria *Staphylococcus aureus* were collected From March 2021 to the end of November 2022, 150 samples of both sexes, ranging in age from 1 to 60 years were randomly selected from 65 male and 85 female patients who had infected burns and wounds at various hospitals. Before to the trials, all of the study's confirmation tests were carried out in the lab, where the diagnosis was verified using the VITEK-2 System. The bacteria were then activated by growing in nutrient broth and cultured for 24 hours at 37 °C to be utilized in studies to determine antibiotic activity.

##### **Antibiotic susceptibility test**

The Kirby-Bauer technique, as specified by the World Health Organization [10], was used to evaluate antibiotic susceptibility for 14 different antibiotics. Picking 1-2 isolated colonies of bacteria from the

original culture and introducing them into a test tube containing 4 ml of normal saline produced a bacterial suspension with moderate turbidity compared to the 0.5 McFarland turbidity standard provides an optical density comparable to the density of a bacterial suspension  $1.5 \times 10^8$  colony forming units (CFU/ml). A portion of the bacterial suspension was transferred and gently and uniformly spread over Mueller-Hinton agar medium, then left for 10 minutes. Following that, the antimicrobial discs were firmly put on the agar to ensure contact with the agar. The plates were then inverted and incubated for 24 hours at 37°C. According to the Clinical Laboratories Standards Institute, inhibition zones formed around the discs were measured in millimetres (mm) using a metric ruler [11].

#### Assessment of biofilm formation

According to instructions to Patel *et al.* [12], *S. aureus* ability to quantitatively produce biofilms was evaluated. All isolates were cultured over-night in Brain Heart Infusion Broth at 37°C. Each isolate was added to tryptic soy broth (TSB), which contains 1% glucose, and well mixed. The turbidity of a suspension of the bacterial isolate was set to McFarland No. 0.5.

To a sterile, 96-well microtiter plate with a flat bottom, a volume (200 µl) of each isolate's culture was added in triplicate. With their covers on, the plate was incubated for 24 hours at 37°C under aerobic conditions. To get rid of the unattached bacteria after the incubation time, the planktonic cells were twice washed with distilled water. 200 µl of 100% methanol was used to fix the adhering bacterial cells in each well for 20 min at room temperature. 200 µl of 0.1% crystal violet was poured into each well and left there for 15 minutes to stain the adherent cells. After the staining process was finished, the additional stain was removed by repeated washing with distilled water (2–3 times). To ensure that the plate was dry, it was dried at room temperature for around 30 minutes. Next, 33% acetic acid was applied to remove the stain.

An ELISA auto reader operating at a wavelength of 630 nm was used to measure optical density (OD) values. All test results were computed, and the average of the OD values of the sterile medium was removed. Cut off value (ODc) was computed, and it may classify isolates as producing biofilms or not [13].

**ODc:** Average OD of negative control + (3 × standard deviation (SD) of Negative control),

**OD isolate:** Average OD of isolate – ODc. By the calculation of cutoff value (ODc), the result of biofilm is detected as below:

**OD ≤ ODc** (no biofilm production).

**ODc < OD ≤ 2 × ODc** (weak biofilm production).

**2 × ODc < OD ≤ 4 × ODc** (moderate biofilm production).

**4 × ODc < OD** (strong biofilm production).

#### Study the antibacterial activity of manganese oxide-nanoparticles

##### Agar well diffusion method

The agar well diffusion method was employed for the determination of this study. Mueller-Hinton agar plates were swabbed (sterile cotton swabs) with broth culture (0.5 McFarland standard) of bacteria. Wells (6 mm diameter) were made in each of these plates using a sterile cork borer. 100 µl from each concentration (32 and 64 mg/ml) of the MnO-NPs were put in each hole by using a micropipette and allowed to diffuse at room temperature for 30 min. The plates were incubated at 37°C for 24 hours. The diameter of any resulting zone of inhibition was measured in millimeters [14].

##### Determination of Minimum Inhibitory Concentration (MIC) of manganese oxide-nanoparticles

The 96-well microtiter plate was used to determine the (MIC) of the MnO-NPs using the broth microdilution technique. The MnO-NPs working solution was prepared in broth at 64 mg/ml, and serial two-fold dilutions of MnO-NPs were prepared directly on the plate to make concentrations of (0.25, 0.5, 1, 2, 4, 8, 16, 32, ) mg/ml. 200 µl of the prepared MnO-NPs put into the first row A wells. In columns, rows B to H contained 100 µl of the broth alone. Using a micropipette, twofold serial dilutions were performed methodically down the columns (from rows A to H). 100 µl was withdrawn from the starting concentrations in row A and transferred to the next row with the 100 µl broth, which was appropriately mixed, and the operation was repeated until the last row (H), when the last 100 µl was discarded. This brings the final volume in all the test wells with the MnO-NPs to 100 µl except the column which had 200 µl of the broth that served as sterility control. 100 µl of the  $1.5 \times 10^8$  CFU/ml bacterial inoculum was transferred into all the wells except the negative control.

Microtiter plates were incubated for 24 hours at 37°C. Following incubation, 20 µl of resazurin dye was added to each well and leave for 30 minutes to see whether any color changes occurred. The Minimum Inhibitory Concentrations of the MnO-NPs at which no color changed from blue to pink in the resazurin broth

test were measured visually in broth micro dilutions [15].

### Study the anti-biofilm activity of manganese oxide-nanoparticles

The anti-biofilm activity of MnO-NPs was tested using a 96-well microtiter plate. The MnO-NPs working solution was created at 32 mg/ml for the MnO-NPs to make the concentrations (32, 16, 8, 4, 2, 1, 0.5 and 0.25) mg/ml. Only the first wells in row A contained 200  $\mu$ l of each sample, whereas rows B through H had 100  $\mu$ l of the broth. Twofold serial dilutions were carried out methodically down the columns (from rows A to H). 100  $\mu$ l was drawn from the starting concentrations in row A and transferred to the next row with the 100  $\mu$ l broth, which was properly mixed, and the operation was repeated until the last row (H), at which time the last 100  $\mu$ l was discarded. Each well received 100  $\mu$ l of the  $1.5 \times 10^8$  CFU/ml bacterial inoculum, with the exception of the negative control. The same procedure as indicated in the paragraph was used (**Assessment of biofilm formation**).

### Statistical analysis

This study employed one-way analysis of variance (ANOVA). Using SPSS version 23, the correlations and significance of the differences were

assessed, and p values  $\leq 0.01$  were used to indicate statistically significant differences. Standard deviation was used to represent the data as mean  $\pm$ .

### Results and Discussion

#### Antibiotic susceptibility test

The results of the current investigation revealed that all *S. aureus* isolates varied in their resistance to the 14 antibiotics utilized in this study, which have been selected in accordance with (CLSI, 2019), which were tested for antibiotic sensitivity (Tabl 1). All (20) bacterial isolates showed resistance to the antibiotics Vancomycin, Azithromycin, and Ceftazidime, with a percentage of 100%. However, the percentage of bacterial resistance to antibiotics Imipenem and Cefotaxime were (90%). Additionally, with percentages of 65%, 55%, and 50%, respectively, the bacterial isolates demonstrated a rather high resistance to the antibiotics Amikacin, Trimethoprim, and Norfloxacin. The bacterial isolates under study recorded a relative sensitivity to some antibiotics, which are Gentamicin and Tobramycin, with a percentage of 65%, respectively, followed by Tetracycline, Ciprofloxacin, Trimethoprim/sulfamethoxazole and Levofloxacin with a percentage of 60%, 55%, 55% and 50%, respectively. Therefore, ten isolates of *S. aureus* that are highly resistant to antibiotics were selected for this study.

**Table (1): Number of isolates and percentage of *Staphylococcus aureus* resistance to a number of antibiotics**

Antibiotics	Symbol	Resistance (R)		Intermediate (I)		Sensitive (S)		Total (%)
		No.	(%)	No.	(%)	No.	(%)	
Cefotaxime (30 $\mu$ g)	CTX	18	90	0	0	2	10	20 (100)
Imipenem (10 $\mu$ g)	IPM	18	90	0	0	2	10	20 (100)
Ciprofloxacin (10 $\mu$ g)	CIP	8	40	1	5	11	55	20 (100)
Levofloxacin (5 $\mu$ g)	LEV	9	45	1	5	10	50	20 (100)
Trimethoprim (10 $\mu$ g)	TM	11	55	1	5	8	40	20 (100)
Amikacin (10 $\mu$ g)	AK	13	65	1	5	6	30	20 (100)
Vancomycin (10 $\mu$ g)	VA	20	100	0	0	0	0	20 (100)
Azithromycin (15 $\mu$ g)	AZM	20	100	0	0	0	0	20 (100)
Tetracycline (10 $\mu$ g)	TE	8	40	0	0	12	60	20 (100)
Gentamicin (10 $\mu$ g)	CN	6	30	1	5	13	65	20 (100)
Ceftazidime (30 $\mu$ g)	CAZ	20	100	0	0	0	0	20 (100)
Norfloxacin (10 $\mu$ g)	NX	10	50	0	0	10	50	20 (100)
Trimethoprim/ sulfamethoxazole (25 $\mu$ g)	SXT	8	40	1	5	11	55	20 (100)
Tobramycin (10 $\mu$ g)	TOB	6	30	1	5	13	65	20 (100)

The current study was considered to be somewhat consistent with some of the results of local and international studies. The researchers, Basil AbdulRazzaq *et al.* [16] found that *Staphylococcus aureus* isolated from different clinical models from

Baghdad hospitals, that this bacterium was resistant to Azithromycin with a percentage of 61.4%, Gentamicin 24%, Levofloxacin 30%, Tetracycline 52.8%, and Vancomycin 14.2%.

### Detection of biofilm formation

Biofilm production is a frequent strategy employed by bacteria to survive under harsh environmental conditions. Bacteria may form biofilms in water systems and on groups of abiotic surfaces often utilized in such systems, as well as in natural

aquatic habitats [17]. The Microtiter plate was used to detect the quantitative of biofilm formation in order to quantify biofilm strength. The findings showed that all isolates had high biofilm formation except for isolates 9 and 10, which had moderate biofilm formation, The 10 best selected isolates as shown in (Table 2).

**Table (2): Biofilm forming of *S. aureus* isolates**

<i>S. aureus</i> isolates	S1	S2	S3	S4	S5	S6	S7	S8	S9	S10
Biofilm forming	Strong	Moderate	Moderate							

(S): *S. aureus* isolates, Control negative (Cut off) = 0.1

### Characterization of manganese oxide-nanoparticles

The following approaches have been used to evaluate the morphological, structural, and optical characteristics of synthesized MnO-NPs:

#### UV-Visible spectroscopy

*Lepidium sativum* aqueous plant leaves extract was combined with  $MnSO_4 \cdot H_2O$ , which caused a change in colour. The stimulation of the metal nanoparticles' generated Surface Plasmon Resonance (SPR) vibrations led to the color shift that was seen. The free electron that results from the conduction and valence bands of metal nanoparticles being near to one another is what causes the SPR. In the synthesize of MnO-NPs, a typical peak value is produced by the collective oscillation of free electrons of metal nanoparticles in resonance with the light wave. The colour shift made it simple to monitor the process and

UV-Vis spectroscopy verified it. Figures 1 and 2 show the UV-Vis spectra of aqueous plant extracts containing MnO-NPs. The modest absorption peak at 300 nm demonstrates the interaction of numerous chemical molecules with mineral ions [18].

The type, size, and morphologies of the NPs generated, the dielectric constant of the medium and temperature, as well as their inter-particle distances, all have a remarkable impact on the surface Plasmon resonance absorbance [19].

Nanoparticles have UV-visible absorption properties [20]. With a rise in NP concentration, the UV-visible absorption intensity of NPs typically rises [21]. In the present study the absorption spectrum was recorded between 250 nm and 1100 nm. In addition, it is observed that the MnO-NPs surface Plasmon resonance band centered at 275 nm in comparison with UV Test for *Lepidium sativum* aqueous plant leaves extract 270 nm.

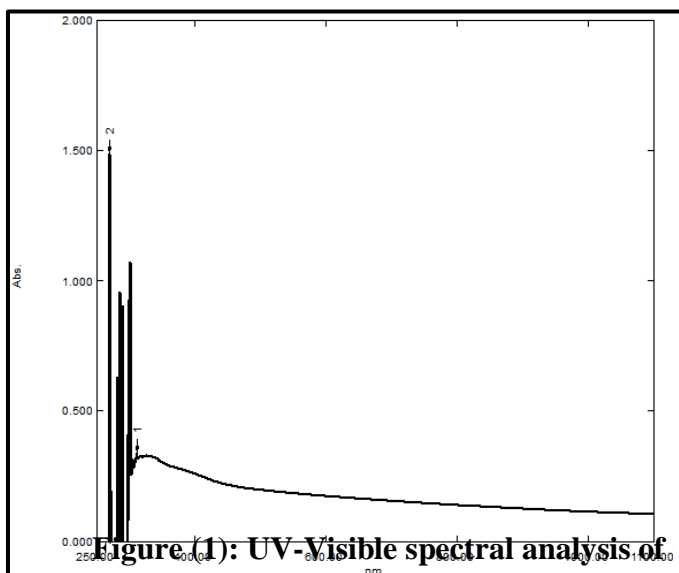


**Figure (1): UV-Visible spectral analysis of *Lepidium sativum* aqueous plant leaves extract**

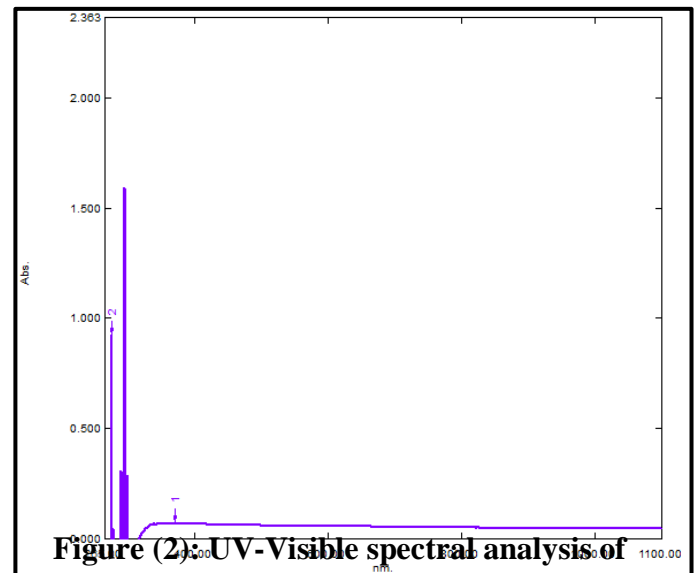


**Figure (2): UV-Visible spectral analysis of MnO-NPs**

### Field emission scanning electron microscopy (FE-SEM)

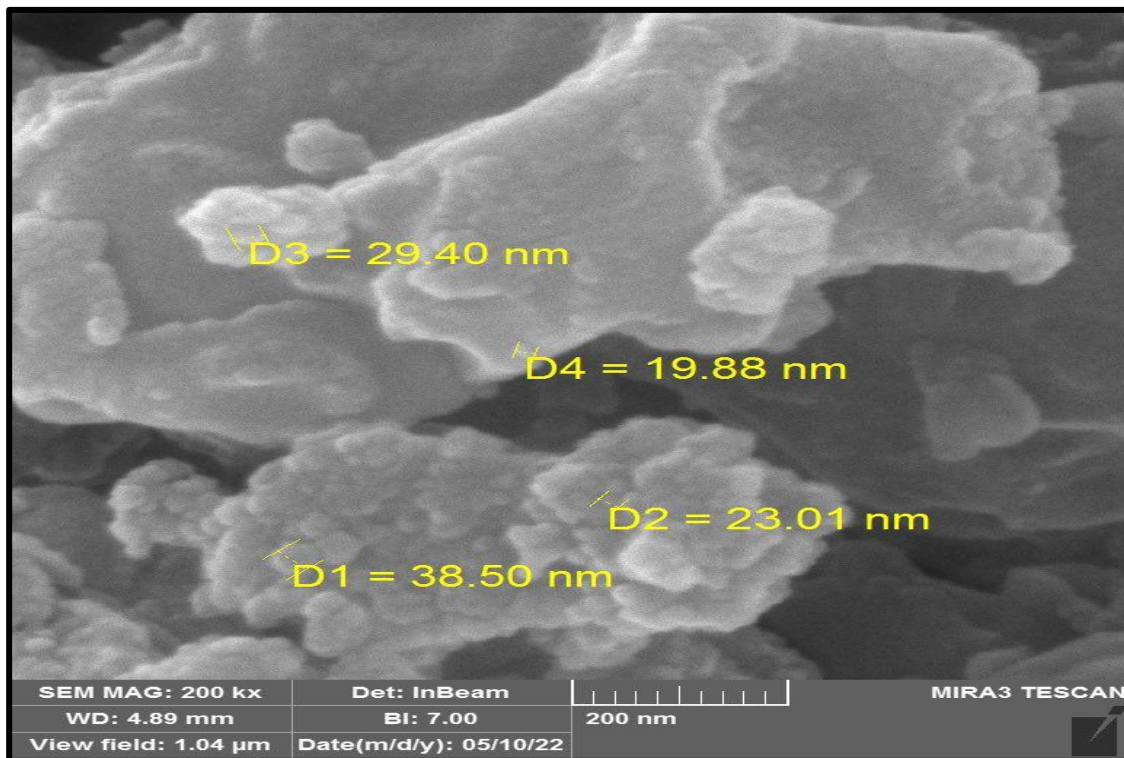
The shape and morphology of the generated green nanoparticles were examined using (FE-SEM), one of the extensively utilized methods for characterizing synthetic nanoparticles. The observations show that nanoparticle morphology is very varied, with a wide range of sizes and shapes.

A Field emission scanning electron microscopy (FE-SEM) has been used to study the surface of MnO-NPs. According to FE-SEM investigation, the particles for MnO-Nps are round and nanoscale in size, Figure 4.

Nanoparticle surface morphology investigations have been carried out using a (FE-SEM). It is widely known that the performance of nanostructure materials is significantly influenced by the surface morphology. The micrographs show that the grain distributions are

uniform. The particles have consistent sizes, a roughly spherical shape, and an average size of around 27.69 nm. The result was in agreement with Ganeshan *et al.* [23] they studied the morphology of the generated MnO-NPs, FE-SEM scans revealed that the particles are virtually spherical with a range of sizes.

This study also agreed with Ogunyemi *et al.* (24) who observed the morphology of the MnO nanoparticles synthesized by chamomile flower extract, and mention the FE-SEM gave a further understanding of the morphology and size details of MnO nanoparticles, and confirmed that MnO nanoparticles were irregularly spherical shaped with the size ranging from 36.6 to 112.0 nm. The majority of MnO-NPs syntheses utilizing plant extracts have been described as being spherical [25], which is consistent with this study also.



### Atomic force microscopy (AFM)

Atomic force microscopy (AFM) research revealed that MnO-NPs were spherical, either individually or in aggregates, in both two- and three-dimensional perspectives, and that the average diameter

particle size for MnO-NPs prepared using *Lepidium sativum* aqueous plant leaves extract was 40.43 nm, Figure 3.

The results were consistent with those of Sinha *et al.* [22] who found that the average MnO-NPs size was determined from an AFM picture.

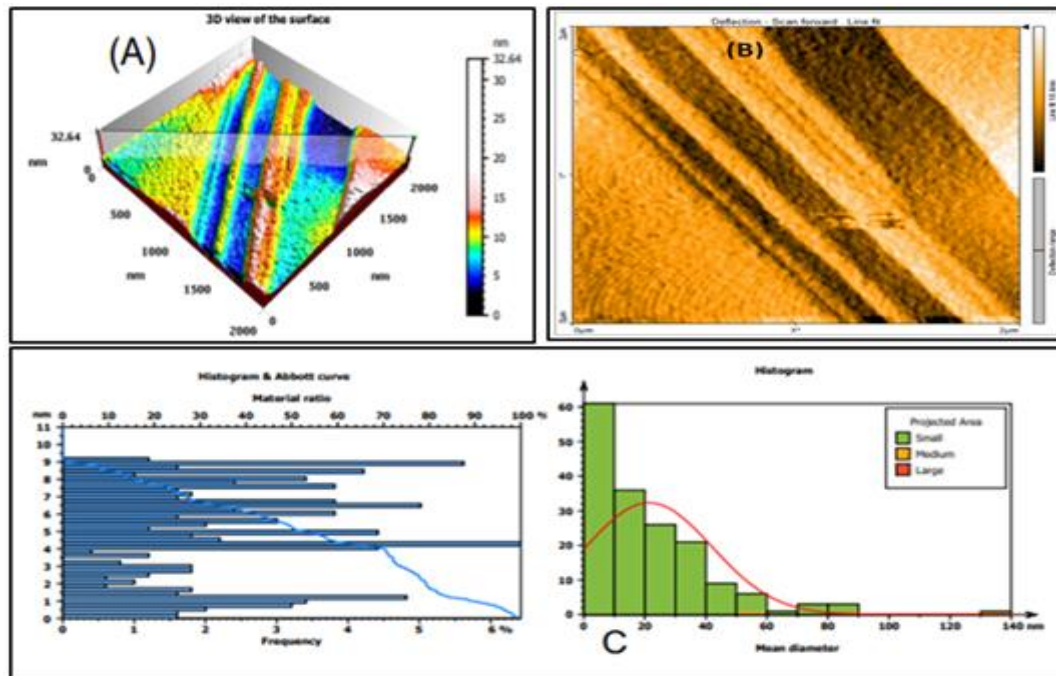


**Figure (3): Atomic force microscopy analysis of MnO-NPs**

**(A): Three-dimensional of MnO-NPs, (B): Two-dimensional of MnO-NPs, (C): AFM diagram of size range of MnO-NPs.**

#### X-ray diffractometer (XRD)

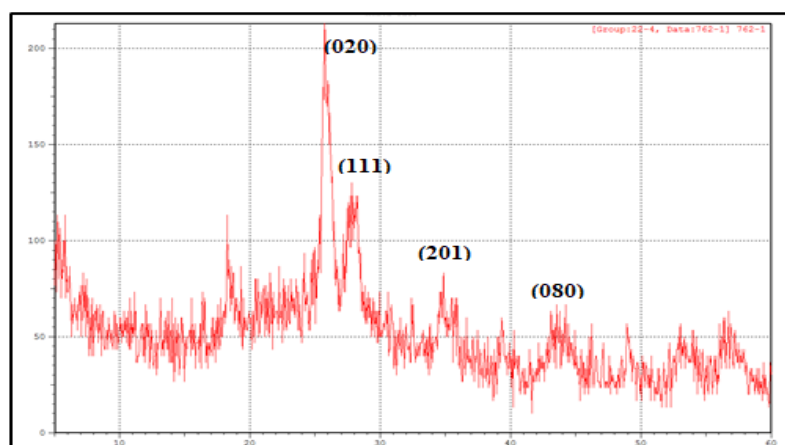
The X-ray diffractometer (XRD) is a powerful technology for crystalline material characterization that offers information on structures, phases, preferred crystal orientations, and other structural factors such as average grain size, crystallinity, strain, and crystal defects [26].

Figure (5) demonstrates the XRD pattern of the MnO-NPs made from aqueous extracts of *Lepidium sativum*. By comparing the XRD peaks to the JCPDS dataset (card No. 04-0326), the (020), (111), (201) and

(080) planes were identified, which amply demonstrates that MnO-NPs are of the orthorhombic system [27]. The Debye-Scherrer formula was used to determine the average crystallite size of the MnO-NPs particles from the XRD peak:

$$D = 0.9\lambda / (\beta \cos\theta)$$

Where  $\lambda$  is the wavelength of X-rays used (1.5405 Å),  $\beta$  is the Full Width Half Maximum (FWHM) in radian and  $\theta$  is the angle of diffraction. The calculated average crystallite size from the XRD peaks for MnO-NPs was found to be 12.68 nm.



**Figure (5): XRD pattern of MnO-NPs**

### Fourier Transform Infrared (FTIR) Spectroscopy Analysis

The most significant and popular analytical technique for determining the presence of particular functional groups in the produced nanomaterial is FTIR spectroscopy [28].

In certain cases, spectra as low as  $400\text{ cm}^{-1}$  ( $25\text{ }\mu\text{m}$ ) were recorded using Fourier Transform Infra-Red (FTIR) spectrophotometers. These spectra were in the range of  $4000\text{ cm}^{-1}$  to  $670\text{ cm}^{-1}$  ( $2.5\text{ }\mu\text{m}$  to  $15\text{ m}$ ). The results of the FTIR Spectra of the *Lepidium sativum* aqueous plant leaves extract revealed the presence of different functional groups such as Phenolic–OH group stretching, C-H stretching, N-H bend, C-C stretching and C-N stretching. The peaks near  $4000$  to  $3200\text{ cm}^{-1}$  and  $2941$  were assigned to O–H stretching and aldehydic C–H stretching, respectively [29], which corresponds to carboxylic acids, primary amines, and alkanes [30]. The peak at  $1641\text{ cm}^{-1}$  is (N-H) due to carbonyl stretching in proteins [31], the peak  $1384\text{ cm}^{-1}$  corresponding to the C–C stretching bond indicates the presence of aromatic compounds and the N–O symmetric stretching that demonstrated the presence of the nitro compounds, respectively [32], the peaks  $1109$  and  $1055$  were assigned to (OH) and (C-H, C-O), respectively [33]. The small peaks situated around  $1000\text{ cm}^{-1}$  represents the presence of ester. The Smallest peaks  $600\text{ cm}^{-1}$  and less indicate the presence of C-Cl stretching of alkyl halides. They had prominent bands of absorbance at peaks ( $3369.14$ ,  $2921.96$ ,  $1608.52$ ,  $1404.08$ , and  $1029.92$ )  $\text{cm}^{-1}$ . In addition, the FTIR Spectra of the  $\text{MnSO}_4\cdot\text{H}_2\text{O}$  had a prominent band of absorbance at peak  $1141.78\text{ cm}^{-1}$ . Moreover, the

FTIR spectroscopy showed that samples analysis had prominent bands of absorbance at peaks ( $619.11$ ,  $1110.92$ ,  $1631.67$  and  $3429.20$ )  $\text{cm}^{-1}$  for the MnO-NPs. The peak ( $1110.92$ ) in the FTIR Spectra of the MnO-NPs is the same peak found in the  $\text{MnSO}_4\cdot\text{H}_2\text{O}$  sample, and was not found in the *Lepidium sativum* aqueous plant leaves extract. Therefore, this indicates the formation of MnO-NPs (Figure 6).

A variety of secondary metabolites found in plants, including terpenoids, sugars, polyphenols, alkaloids, proteins, and phenolic acids, are essential for the creation of metal nanoparticles [34].

Results indicate that metal nanoparticles may bind to free carbonyl groups in amino acid residues of proteins found in plant leaf extract while encasing or capping the latter to avoid their aggregation. Certain biological components, including proteins, can reduce metal ions while also stabilizing metal nanoparticles in an aqueous environment. Shankar *et al.* [35] discovered proteins and secondary metabolites in the water-soluble fractions of Geranium leaves and proved that terpenoids contribute to metal ion reduction and metal ion oxidation to carbonyl groups. According to FTIR study, the chlorophyll ester C=O group acts as a reducing agent, while another protein is involved in the surface capping of metal nanoparticles of Geranium leaf extract. Proteins and other ligands contained in plant extracts were discovered to be responsible for the creation and stability of nanoparticles [36].

The results were similar to Ogunyemi *et al.* [24], who used FTIR to identify functional groups in MnO-NPs produced from *Matricaria chamomilla* L. leaf extract.

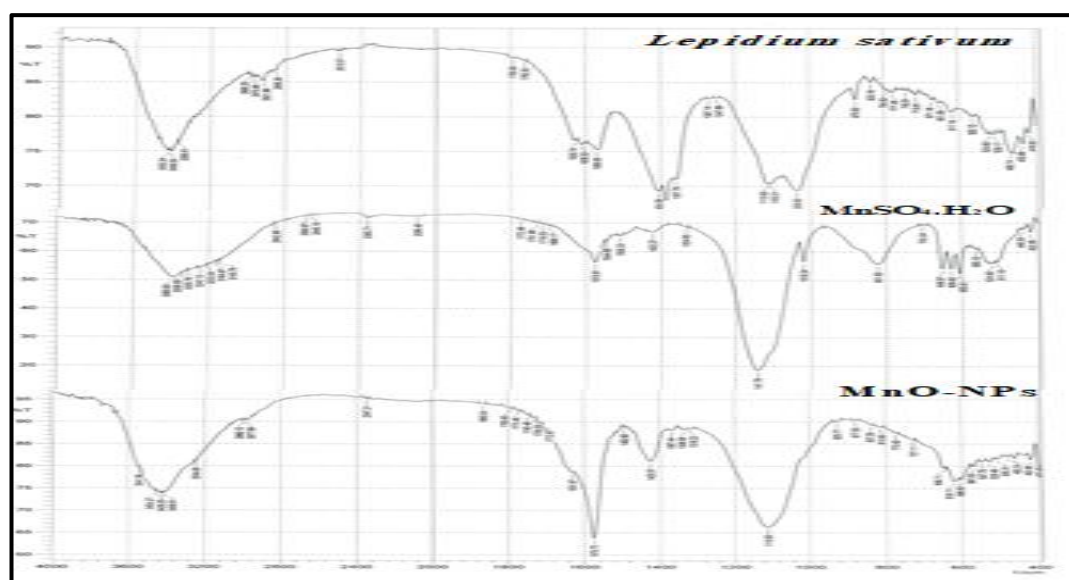


Figure (6): FTIR Spectra Pattern of *Lepidium sativum* aqueous plant leaves extract,  $\text{MnSO}_4\cdot\text{H}_2\text{O}$  and MnO-NPs

**Antibacterial activity of manganese oxide-nanoparticles**

**Well diffusion method**

The well-diffusion method evaluated the antibacterial activity of the nanoparticles used in this study on *S. aureus*. The results showed that the MnO-NPs in concentrations 64 mg/ml was more effective than the MnO-NPs in concentrations of 32 mg/ml, which gave the highest inhibition zone  $19.67 \pm 0.57$  and  $15.00 \pm 1.00$  mm, respectively, the *S. aureus*

isolate 6, with a significant difference ( $P \leq 0.01$ ), as seen in (Tables 3).

Metal nanoparticles' true antibacterial activity's exact mechanism is still unclear. There are, however, a number of papers outlining the potential mechanism behind its antibacterial action. It has been discovered that the antibacterial activity of metal nanoparticles greatly depends on a number of factors, including the particle's size, shape, and surface charge [37]. The size, shape, dose, stability, morphology, and duration of therapy are the primary factors that determine the antibacterial capability of nanoparticles [38].

**Table (3): Antibacterial activity of MnO-NPs on *S. aureus* isolate**

No of isolates	Mn-NPs		LSD value
	32 mg/ml	64 mg/ml	
S <sub>1</sub>	14.33±0.57	19.67±0.57	2.170**
S <sub>2</sub>	14.33±0.57	19.67±0.57	2.170**
S <sub>3</sub>	7.33±0.57	9.67±0.57	2.170**
S <sub>4</sub>	10.67±0.57	14.33±0.57	3.432**
S <sub>5</sub>	11.67±0.57	15.33±0.57	2.170**
S <sub>6</sub>	15.00±1.00	19.67±0.57	3.069**
S <sub>7</sub>	12.67±0.57	15.67±0.57	2.170**
S <sub>8</sub>	12.67±0.57	17.33±0.57	2.170**
S <sub>9</sub>	13.33±0.57	15.67±0.57	2.170**
S <sub>10</sub>	13.67±0.57	16.33±0.57	2.170**
LSD value	1.469**	1.341**	-----
**( $P \leq 0.01$ )			

(S): *S. aureus*

The numbers in the table mention to inhibition zone measured in (mm)

Manganese oxide-nanoparticles affect bacteria by causing direct contact of MnO nanoparticles with the bacterial membrane due to their special sheet-like structure; producing reactive oxygen species; and causing membrane damage, leakage of electrolytes and intracellular contents, and a decrease in ATPase activity, all of which contribute to bacterial death [39].

According to studies, MnO NPs exhibited an antibacterial impact on bacteria with varied inhibitory zone diameters, including *S. aureus*, *E. coli*, *Klebsiella pneumonia*, *B. subtilis* and *Pseudomonas aeruginosa* [40]. MnO NPs were also observed to have a greater inhibitory impact on Gram-positive bacteria than on

Gram-negative bacteria [41]. Many studies have demonstrated that the physical (such as lipid molecule disintegration) and chemical (such as oxidative stress) degradation play a major role in the antibacterial impact of nanomaterials [39]. This study agreed with Saod *et al.* [42], According to their study's findings, MnO-NPs had inhibitory zones of 12, 14, and 18 mm for *P. aeruginosa*, *K. pneumoniae* and *E. coli*, respectively.

### Determination of the (MIC) of the manganese oxide-nanoparticles

The MIC of the nanoparticles was ascertained utilizing the 96-well microtiter plate and the broth microdilution technique. The MIC of the antibacterial agent *S. aureus* has been established using a technique utilizing the oxidation-reduction colorimetric indicator resazurin. Resazurin may be easily seen with the naked eye and the MIC can be established even without the use of a spectrophotometer. Resazurin is blue in its oxidized state but becomes pink when reduced by living cells [43].

The result of The MIC values of the MnO-NPs on *S. aureus* isolates 1, 2, 6 and 8 were 1 mg/ml while in isolation 3, 7, 9 and 10, was 2 mg/ml, and in isolation 4

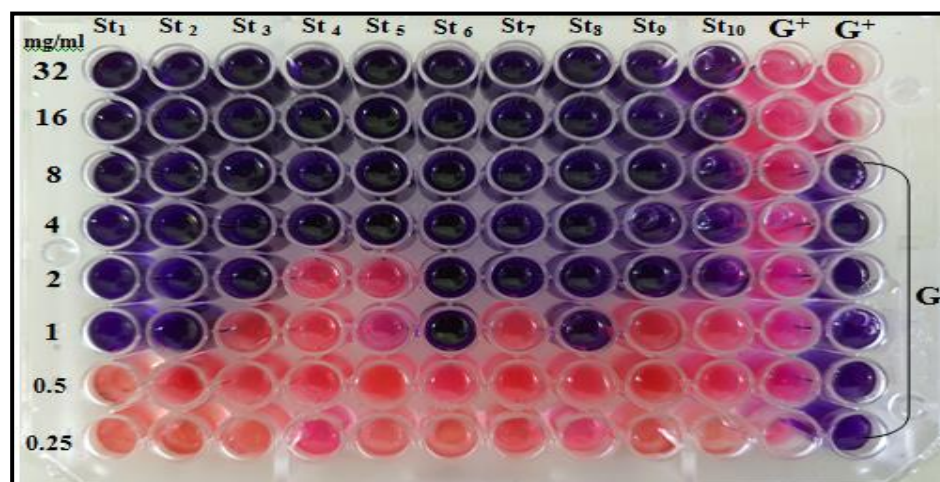
and 5 was 4 mg/ml, as shown in (Tables 4) and (Figure 7).

This result shows that the MnO-NPs utilized in this work had efficiency that was concentration dependent, which is consistent with reports of other metal oxide nanoparticles from other studies. [44]. Also, it has been shown that the sizes of nanoparticles significantly influence how effective they are against bacterial [45]. This nanoscale size has a variety of morphologies with large surface area, charge, adsorption, and chemical reactivity that allow them to interact with biological systems effectively and inhibit them significantly [46]. As a result, we infer that the nanoscale diameters of MnO-NPs were critical to their antibacterial efficacy. The 10 best selected isolates as shown in table(4).

**Table (4): MIC of MnO-NPs on *S. aureus* isolate**

Isolate	S1	S2	S3	S4	S5	S6	S7	S8	S9	S10
Mn-NPs										
MIC mg/ml	1	1	2	4	4	1	2	1	2	2

(S): *S. aureus*



(Media only)

**Figure (7): MIC of MnO-NPs on *S. aureus* isolate**

The results of this study agree with Azhir *et al.* [47], they found that the nanoparticles exhibited efficient antibacterial activity against both Gram positive and Gram negative bacteria, which was validated through the broth microdilution method. Furthermore, Packirisamy *et al.* [48] revealed *B. subtilis*, *E. coli* and *P. aeruginosa* susceptible to NPs as anti-

microbial activity and the susceptible increased by increasing the concentration.

In another work, Kamran *et al.* [49] synthesized manganese oxide-nanoparticles using *Cinnamomum verum* bark extract and evaluated their antimicrobial activity on *Escherichia coli* and *Staphylococcus aureus*. The natural compounds present in the bark helped in the synthesis

of manganese oxide-nanoparticles and produced effective antimicrobial activity against the above-mentioned strains.

### Anti-Biofilm activity of manganese oxide-nanoparticles

A tightly packed group of microbial cells known as a biofilm attaches to and develops on living or nonliving surfaces, and it surrounds itself with secreted polymers. Due to treatment resistance, biofilm-associated infections are sometimes difficult to treat [50]. Thus, it is crucial to find novel and potent compounds that prevent the development of bacterial biofilms.

Manganese oxide-nanoparticles inhibited 100% of the biofilm formation of *S. aureus* in 1 mg/ml, as shown in (Table 5).

The development of biofilms has been linked to bacteria's development of antibiotic resistance [51].

When exposed to MnO-NPs, biofilm formation was lost, which suggests virulence when interacting with and colonizing host tissue. The observed reduction of biofilm development is in line with research by Cai *et al.* [52], who showed that the capacity to suppress biofilm formation and bacterial motility depend on concentration.

Bacterial biofilms are widespread and develop across a number of phases [53]. Mn (II) complexes can prevent the development of biofilms in two different ways: I when planktonic bacteria attach to a surface and begin to form a micro-colony; and (ii) when the metabolism of a community enclosed in an extracellular matrix is perturbed [54, 55].

This study agreed with Ogunyemi *et al.*[44] which mention the MnO NPs synthesized using chamomile extract are an efficient anti-biofilm agent.

**Table (5): Biofilm formation of *S. aureus* before and after treatment with MnO-NPs**

No of isolates	Before treatment (control)	After treatment (Mn NPs mg/ml)							
		0.25	0.5	1	2	4	8	16	32
S1	Strong	Weak	Weak	No Biofilm					
S2	Strong	Weak	No Biofilm						
S3	Strong	Moderate	Weak	No Biofilm					
S4	Strong	Weak	Weak	No Biofilm					
S5	Strong	Weak	No Biofilm						
S6	Strong	Weak	Weak	No Biofilm					
S7	Strong	Weak	Weak	No Biofilm					
S8	Strong	Moderate	Weak	No Biofilm					
S9	Moderate	Moderate	Weak	No Biofilm					
S10	Moderate	Weak	Weak	No Biofilm					

(S): *S. aureus*, Control negative (cut off) = 0.1

### Conclusion

According to the results of the current study, it can be concluded that the green synthesize method is a successful method to prepare MnO-NPs, and the synthesized MnO-NPs have significant antibacterial *S. aureus* agent, it also inhibits of the formation biofilms in *S. aureus* depending on the concentration used.

### References

1. Khan, S. A., Shahid, S., and Lee, C.-S. S. (2020). Green synthesis of gold and silver

nanoparticles using leaf extract of *Clerodendrum inerme*; characterization, antimicrobial, and antioxidant activities. *Biomol. Ther.* 10:835. doi: 10.3390/biom10060835.

2. Khan, S. A., Shahid, S., Mahmood, T., and Lee, C.-S. (2021). Contact lenses coated with hybrid multifunctional ternary nanocoatings (Phytomolecule-coated ZnO nanoparticles:Gallic acid:tobramycin) for the treatment of bacterial and fungal

- keratitis. *Acta Biomater.* 128, 262–276. doi: 10.1016/j.actbio.2021.04.014.
3. Khan, S. A., and Lee, C. S. (2020). Recent progress and strategies to develop antimicrobial contact lenses and lens cases for different types of microbial keratitis. *Acta Biomater.* 113, 101–118. doi: 10.1016/j.actbio.2020.06.039.
  4. Joshi, N. C., and Prakash, Y. A. S. H. W. A. N. I. (2019). Leaves extract-based biogenic synthesis of cupric oxide nanoparticles, characterizations, and antimicrobial activity. *Asian J Pharm Clin Res*, 12(8), 288–291.
  5. Al-Khafaji, A. R. and AL-Azawi, A. H. (2022). Green Method Synthesis of Silver Nanoparticles Using Leaves Extracts of *Rosmarinus officinalis*. *Iraqi Journal of Biotechnology*, 21(2): 251-267.
  6. Annu, A. A., and Ahmed, S. (2018). Green synthesis of metal, metal oxide nanoparticles, and their various applications. *Handbook of Ecomaterials, 2018*, 1-45.
  7. Sour, M., Hoseinpour, V., Shakeri, A., and Ghaemi, N. (2018). Optimisation of green synthesis of MnO nanoparticles via utilising response surface methodology. *IET nanobiotechnology*, 12(6), 822-827.
  8. Srihasam, S., Thyagarajan, K., Korivi, M., Lebaka, V. R., and Mallem, S. P. R. (2020). Phytogenic generation of NiO nanoparticles using Stevia leaf extract and evaluation of their in-vitro antioxidant and antimicrobial properties. *Biomolecules*; 10(1), 89.
  9. Ezhilarasi, A. A., Vijaya, J. J., Kaviyarasu, K., Kennedy, L. J., Ramalingam, R. J. and Al-Lohedan, H. A. (2018). Green synthesis of NiO nanoparticles using Aegle marmelos leaf extract for the evaluation of in-vitro cytotoxicity, antibacterial and photocatalytic properties. *Journal of Photochemistry and Photobiology B: Biology*; 180, 39-50.
  10. World Health Organization (WHO). (2003). Basic laboratory procedures in clinical bacteriology. 2<sup>nd</sup> ed. Geneva, Switzerland.
  11. Clinical Laboratory Standards Institute (CLSI). (2019). Performance Standards for Antimicrobial Susceptibility Testing; CLSI Supplement, CLSI M100-28th ed., Clinical and Laboratory Standards Institute Wayne, PA, U.S.A. 39(1).
  12. Patel, F. M., Goswami, P. N. and Khara, R. (2016). Detection of Biofilm formation in device associated clinical bacterial isolates in cancer patients. *Sri Lankan Journal of Infectious Diseases*, 6(1). 43-50.
  13. Kırmusaoğlu, S. (2019). The methods for detection of biofilm and screening antibiofilm activity of agents. *Antimicrobials, antibiotic resistance, antibiofilm strategies and activity methods*, 7. 1-17. DOI: [http:// dx.doi.org / 10.5772 / intechopen.84411](http://dx.doi.org/10.5772/intechopen.84411).
  14. Valgas, C.; de Souza, S. M.; Smânia, E. F. A. and Smânia, A. (2007). Screening methods to determine antibacterial activity of natural products. *Braz. J. Microbiol.*, 38: 369–380.
  15. Ohikhena, F. U.; Wintola, O. A. and Afolayan, A. J. (2017). Evaluation of the Antibacterial and Antifungal Properties of *Phragmanthera capitata* (Sprengel) Balle (Loranthaceae), a Mistletoe Growing on Rubber Tree, Using the Dilution Techniques. *The Scientific World Journal*, Article ID 9658598. 8 pages doi.org/10.1155/2017/9658598.
  16. Basil AbdulRazzaq, A., Shami, A. M., and Ghaima, K. K. (2022). Detection of vanA and vanB genes Among Vancomycin Resistant *Staphylococcus aureus* Isolated from Clinical Samples in Baghdad Hospitals. *Iraqi journal of biotechnology*, 21(1).
  17. Bronowskil, C. James, C. E. and Winstanley, C. (2014). Role of environmental survival in transmission of campylobacter jejuni. *FEMS Microbiol. Lett.*, 356(1). 8-19.
  18. Femi-Adepoju, A. G.; Dada, A. O.; Otun, K. O.; Adepoju, A. O. and Fatoba, O. P. (2019). Green synthesis of silver nanoparticles using terrestrial fern (*Gleichenia Pectinata* (Willd.) C. Presl.): characterization and antimicrobial studies. *Heliyon*, 5(4): e01543.
  19. Mahmoud, M. A.; Chamanzar, M.; Adibi, A. and El-Sayed, M. A. (2012). Effect of the dielectric constant of the surrounding medium and the substrate on the surface plasmon resonance spectrum and sensitivity factors of highly symmetric systems: silver nanocubes. *Journal of the American Chemical Society*. 134(14): 6434-6442.
  20. Kumar, V. and Yadav, S. K. (2009). Plant-mediated synthesis of silver and gold nanoparticles and their applications. *Journal of Chemical Technology & Biotechnology: International Research in Process, Environmental & Clean Technology*, 84(2), 151-157.

21. Kumar, V. and Yadav, S. K. (2013). Influence of physiochemical factors on size of gold nanoparticles synthesised using leaf extract of *Syzygium cumini*. *Journal of Chemical Science and Technology*, 2(1), 104-107.
22. Sinha, A., Singh, V. N., Mehta, B. R., and Khare, S. K. (2011). Synthesis and characterization of monodispersed orthorhombic manganese oxide nanoparticles produced by *Bacillus* sp. cells simultaneous to its bioremediation. *Journal of hazardous materials*, 192(2), 620-627.
23. Ganeshan, S., Ramasundari, P., Elangovan, A., Arivazhagan, G., and Vijayalakshmi, R. (2017). Synthesis and characterization of MnO<sub>2</sub> nanoparticles: study of structural and optical properties. *Int J Sci Res Phys Appl Sci*, 5(6), 5-8.
24. Ogunyemi, S. O., Fang, Y., Qiu, W., Li, B., Chen, J., Yang, M., and Sun, G. (2019). Role of type IV secretion system genes in virulence of rice bacterial brown stripe pathogen *Acidovorax oryzae* strain RS-2. *Microbial pathogenesis*, 126, 343-350.
25. Moon, S. A., Salunke, B. K., Saha, P., Deshmukh, A. R., and Kim, B. S. (2018). Comparison of dye degradation potential of biosynthesized copper oxide, manganese dioxide, and silver nanoparticles using *Kalopanax pictus* plant extract. *Korean Journal of Chemical Engineering*, 35(3), 702-708.
26. Salari, S.; Bahabadi, S.E.; Samzadeh-Kermani, A. and Yosefzaei, F. (2019). In-vitro evaluation of antioxidant and antibacterial potential of green synthesized silver nanoparticles using *Prosopisfarcta* fruit extract. *Iranian Journal of Pharmaceutical Research*, 18 (1): 430-445.
27. Jang, Y. S., Kim, J. H., Lee, J. K., Park, B. K., and Kang, Y. C. (2012). Electrochemical properties of 0.6 Li<sub>2</sub>MnO<sub>3</sub>· 0.4 Li (Ni<sub>0.8</sub>Co<sub>0.15</sub>Al<sub>0.05</sub>)O<sub>2</sub> composite nanopowders prepared by spray pyrolysis. *Int. J. Electrochem. Sci*, 7, 12370-12382.
28. Fouad H, Li HJ, Hosni D, *et al.* (2018) Controlling *Aedes albopictus* and *Culex pipiens pallens* using silver nanoparticles synthesized from aqueous extract of *Cassia fistula* fruit pulp and its mode of action. *Artif Cells Nanomed Biotechnol*. 46:558–567.
29. Saheed, Y.; Umar, A.F. and Iiyasu, M.Y. (2020). Potential of silver nano particles synthesized from *Ficus sycomorus* Linn against multidrug resistant *Shigella* species isolated from clinical specimens. *American Journal of Life Sciences*, 8(4): 82-90.
30. Pandey, A.; Sharma, S.K.; Singh, L. and Singh, T. (2013). An overview on *Desmostachya bipinnata*. *J. Drug Discov. Ther.*, 7:67–68.
31. Singh, A.; Mittal, S.; Shrivastava, R.; Dass, S. and Srivastava, J.N. (2012). Biosynthesis of silver nanoparticles using *Ricinus communis* leaf extract and its antibacterial activity. *Digest Journal of Nanomaterials and Biostructures*, 7(3): 1157–1163.
32. Bhumi ,G.; LingaRao, M. and Savithamma N. (2015). Green synthesis of silver nanoparticles from the leaf extract of *Adhoda vasicanes* and assessment of its antibacterial activity. *Asian J. Pharm. Clin. Res.*, 8:62–67.
33. Hadjiivanov, K.I.; Panayotov, D.A.; Mihaylov, M.Y.; Ivanova, E.Z.; Chakarova, K.K.; Andonova, S.M. *et al.* (2021). Power of infrared and raman spectroscopies to characterize metal organic frameworks and investigate their interaction with guest molecules. *Chemical Review*, 121:1286-1424.
34. Kuppusamy, P., Yusof, M.M., Maniam, G.P. and Govindan, N. (2014). Biosynthesis of metallic nanoparticles using plant derivatives and their new avenues in pharmacological applications—an updated report. *Saudi Pharm. J.* 8, 473–484.
35. Shankar, S.S., Ahmad, A., Pasricha, R. and Sastry, M. (2003). Bioreduction of chloroaurate ions by geranium leaves and its endophytic fungus yields gold nanoparticles of different shapes. *J. Mater. Chem.* 13, 1822–1826.
36. Mude, N., Ingle, A., Gade, A., Rai, M. (2009). Synthesis of silver nanoparticles using callus extract of *Carica papaya*-a first report. *J. Plant Biochem. Biotechnol.* 18, 83–86.
37. Dakal, T. C., Kumar, A., Majumdar, R. S., & Yadav, V. (2016). Mechanistic basis of antimicrobial actions of silver nanoparticles, *Front. Microbiol.* 7 (2016).
38. Jesudoss, S. K., Vijaya, J. J., Selvam, N., Kombaiyah, K., Sivachidambaram, M., Adinaveen, T. and Kennedy, L. J. (2016). Effects of Ba doping on structural, morphological, optical, and photocatalytic properties of self-assembled ZnO

- nanospheres. *Clean Technologies and Environmental Policy*, 18(3), 729-741.
39. Du, T., Chen, S., Zhang, J., Li, T., Li, P., Liu, J., and Wang, S. (2020). Antibacterial activity of manganese dioxide nanosheets by ROS-mediated pathways and destroying membrane integrity. *Nanomaterials*, 10(8), 1545.
  40. Cherian, E., Rajan, A., and Baskar, G. (2016). Synthesis of manganese dioxide nanoparticles using co-precipitation method and its antimicrobial activity. *International Journal of Modern Science and Technology*, 1(01), 17-22.
  41. Manjula, R., Thenmozhi, M., Thilagavathi, S., Srinivasan, R., and Kathirvel, A. (2020). Green synthesis and characterization of manganese oxide nanoparticles from *Gardenia resinifera* leaves. *Materials Today: Proceedings*, 26, 3559-3563.
  42. Saod, W. M., Hamid, L. L., Alaallah, N. J., and Ramizy, A. (2022). Biosynthesis and antibacterial activity of manganese oxide nanoparticles prepared by green tea extract. *Biotechnology Reports*, 34, e00729.
  43. Ncube, N. S.; Afolayan, A. J. and Okoh, A. I. (2008). Assessment techniques of antimicrobial properties of natural compounds of plant origin: current methods and future trends. *African Journal of Biotechnology*, 12(7): 1797-1806.
  44. Ogunyemi, S. O., Zhang, F., Abdallah, Y., Zhang, M., Wang, Y., Sun, G. *et al.* (2019). Biosynthesis and characterization of magnesium oxide and manganese dioxide nanoparticles using *Matricaria chamomilla* L. extract and its inhibitory effect on *Acidovorax oryzae* strain RS-2. *Artificial cells, nanomedicine, and biotechnology*, 47(1), 2230-2239.
  45. Król, A., Pomastowski, P., Rafińska, K., Railean-Plugaru, V. and Buszewski, B. (2017). Zinc oxide nanoparticles: Synthesis, antiseptic activity and toxicity mechanism. *Advances in colloid and interface science*, 249, 37-52.
  46. Wang, L., Hu, C. and Shao, L. (2017). The antimicrobial activity of nanoparticles: present situation and prospects for the future. *International journal of nanomedicine*, 12, 1227.
  47. Azhir, E., Etefagh, R., Mashreghi, M., and Pordeli, P. (2015). Preparation, characterization and antibacterial activity of manganese oxide nanoparticles. *Physical Chemistry Research*, 3(3), 197-204.
  48. Packirisamy, R. G., Govindasamy, C., Sanmugam, A., Karuppasamy, K., Kim, H. S., and Vikraman, D. (2019). Synthesis and antibacterial properties of novel ZnMn<sub>2</sub>O<sub>4</sub>-chitosan nanocomposites. *Nanomaterials*, 9(11), 1589.
  49. Kamran, U., Bhatti, H. N., Iqbal, M., Jamil, S., and Zahid, M. (2019). Biogenic synthesis, characterization and investigation of photocatalytic and antimicrobial activity of manganese nanoparticles synthesized from *Cinnamomum verum* bark extract. *Journal of Molecular Structure*, 1179, 532-539.
  50. Kumar, L., Chhibber, S. and K. (2013). Harjai, Zinger one inhibits biofilm formation and improve Antibiofilm efficacy of ciprofloxacin against *Pseudomonas aeruginosa* PAO1. *Fitoterapia*, 90, 73-78.
  51. Rajkumari, J., Busi, S., Vasu, A. C. and Reddy, P. (2017). Facile green synthesis of baicalein fabricated gold nanoparticles and their antibiofilm activity against *Pseudomonas aeruginosa* PAO1. *Microbial pathogenesis*, 107, 261-269.
  52. Cai, L., Chen, J., Liu, Z., Wang, H., Yang, H. and Ding, W. (2018). Magnesium oxide nanoparticles: effective agricultural antibacterial agent against *Ralstonia solanacearum*. *Frontiers in microbiology*, 9, 790.
  53. Patel, I., Patel, V., Thakkar, A., and Kothari, V. (2014). Microbial biofilms: microbes in social mode. *International Journal of Agricultural and Food Research*, 3(2).
  54. Jabłońska-Wawrzycka, A., Rogala, P., Czerwonka, G., Michałkiewicz, S., Hodorowicz, M., Gaczyńska, K., ... and Kowalczyk, P. (2021). Tuning Anti-Biofilm Activity of Manganese (II) Complexes: Linking Biological Effectiveness of Heteroaromatic Complexes of Alcohol, Aldehyde, Ketone, and Carboxylic Acid with Structural Effects and Redox Activity. *International journal of molecular sciences*, 22(9), 4847.
  55. Al-Khafaji, A. R. and AL-Azawi, A. H. (2022). The Phenolic Compounds Extracted From *Rosmarinus officinalis* L. and Effect of on The Biofilm Genes in *Pseudomonas aeruginosa*. *Ann. For. Res.*, 65(1): 1943-1958.